Influence of Niobium on Structure/Property Relationships in C-Mn Shipbuilding Steel

V.P. Deshmukh, S.B. Yadaw, A.K. Shah, and D.K. Biswas

The effect of niobium microaddition in C-Mn steel on microstructure, tensile properties, ductile-brittle transition temperature, and weldability have been investigated. Niobium microaddition adversely affects the transition temperature and toughness of the heat-affected zone, counteracting its favorable effects of refined grain size and low inclusion and pearlite content.

Keywords

C-Mn steel, ductile-brittle transition temperature, heat-affected zone simulation, microstructure, niobium microalloying, tensile properties

1. Introduction

CONVENTIONAL C-Mn steels that contain up to 0.2% C and 1.5% Mn are used in many engineering applications. This steel, in the hot-rolled and normalized condition, is also used for ship hull construction, as it possesses an optimum combination of strength, low-temperature notch toughness, weldability, and formability.

The advent of microalloyed steel technology brought an improvement in yield strength and toughness properties of low-alloy steels through controlled rolling. These steels are now being used in many structural applications, replacing conventional high-strength, low-alloy steels. However, the use of microalloyed steels in the shipbuilding industry has not yet found wide acceptance. This is probably due to conflicting reports in the literature (Ref 1-3) about the low-temperature toughness and weldability aspects of these steels.

The principal objective of this work was to study the influence of niobium microaddition in controlled rolled C-Mn steel on the microstructural, tensile, and impact transition temperature properties of this material. Of particular interest was heat-affected zone (HAZ) toughness.

2. Experimental Method

2.1 *Materials*

Two steels were studied; their chemical compositions are given in Table 1. The first steel, designated C-Mn, was made in 12 mm thick plates in the hot-rolled and normalized condition. This was used as a reference material. In the other steel, designated C-Mn-Nb, 0.03% Nb was added with lower carbon content. This composition was designed to achieve desired improvement in strength, toughness, and weldability as compared to plain C-Mn steel. This steel was produced through a LD/vacuum arc degassing/continuous casting route and was controlled rolled to 12 mm thick plate with a minimum 12% reduction in the final two passes in the temperature range of 920 to 800 °C.

V.P. Deshmukh, A.K. Shah and D.K. Biswas, Naval Materials Research Laboratory, Naval Dockyard, Bombay, India; **S.B. Yadav,** Defence Materials and Stores Research and Development Establishment, Kanpur, India

2.2 *Metallography*

Polished and etched samples were prepared for evaluation of microstructural parameters such as grain size, pearlite volume fraction, and inclusion content using a LECO (Leco Corp., St. Joseph, MI) automatic image analyzer. Identification and analysis of inclusions were carried out using a scanning electron microscope (SEM) equipped with an energy-dispersive x-ray (EDX) analyzer.

Transmission electron microscopy (TEM) studies were performed using thin foils. For this purpose, thin slices (0.2 mm) were cut in a transverse-longitudinal (T-L) orientation using a Buehler (Buehler, Ltd., Lake Bluff, IL) isomet slow-speed saw. These slices were mechanically ground to a 0.1 mm thickness. Disks with a diameter of 3 mm were then punched from the ground slices and electropolished in a Fischione (Fischione, E.A., Instruments, Inc., Export, PA) twin-jet polisher using an electrolyte of 10% perchloric acid and 90% acetic acid at 10 °C. A polishing voltage of 12 V was maintained. The thin foils were examined using a JEOL 200CX TEM operating at 160 kV.

2.3 *Testing*

Tensile testing was performed at room temperature according to ASTM standard E 8 (Ref 4). Yield strength (YS), ultimate tensile strength (UTS), percentage elongation (%E), and ratio of yield strength to ultimate tensile strength (YS/UTS) results were obtained for both steels. Average values were determined by testing a minimum of three samples for each steel. Charpy impact testing was carried out per ASTM standard E 23 (Ref 5)

Table 1 Chemical compositions of experimental steels

Element, wt%	Steel	
	C-Mn	C-Mn-Nb
Carbon	0.16	0.11
Manganese	1.40	1.20
Silicon	0.27	0.26
Phosphorus	0.017	0.015
Sulfur	0.014	0.010
Aluminum	0.035	0.020
Niobium	...	0.030
Nitrogen	0.0047	0.0068

on longitudinal-transverse (L-T) oriented V-notch specimens at temperatures ranging from room temperature to −80 °C. Ductile-to-brittle transition temperature (DBTT) curves were generated from these impact energy values. The DBTT was defined at a temperature corresponding to an impact energy value of 20 J.

2.4 *Weldability*

Weldability aspects of the steels were studied in terms of HAZ toughness. In a real weld joint, the HAZ is relatively thin and irregular in shape. This geometry is very difficult to test by standard methods to get a true picture of HAZ properties. To solve this problem, Charpy-sized sample blocks of both the steels were treated for HAZ simulation using a Smitweld thermal cycle simulator. Thermal cyclings were given with a peak temperature of 1250 °C and cooled at different rates from 800 to 500 °C to achieve desired heat inputs of 1.6, 3.4, and 4.5 kJ/mm. These heat inputs were selected to cover the typical heat inputs in manual metal-arc and submerged-arc welding practice followed in ship construction. Simulated samples were then V-notched in the L-T orientation for impact testing. Impact energy testing was carried out only at −30 °C due to the limited availability of simulated samples. Microhardness measurements were also carried out on simulated HAZ samples using a Vickers microhardness tester.

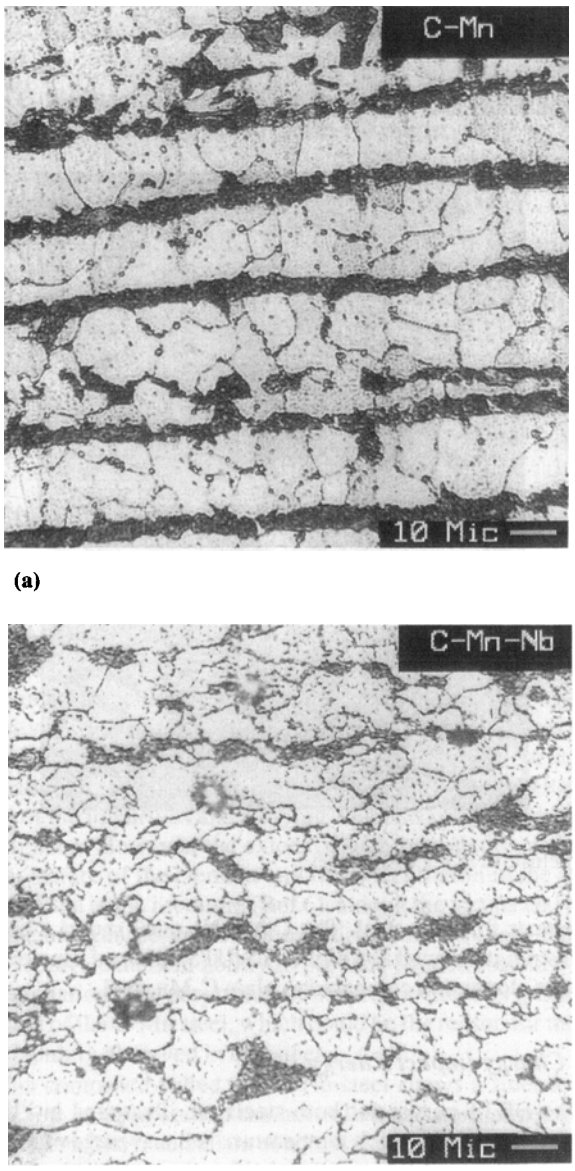

Fig. 1 Video-optical micrographs. (a) C-Mn. (b) C-Mn-Nb

3. Results

3.1 *Microstructural Characterization*

Video-optical micrographs of both steels are shown in Fig. 1. The light and dark phases in the micrographs are ferrite and pearlite, respectively. Severe pearlite banding was observed in plain C-Mn steel. Pearlite and ferrite volume fractions and ferrite grain-size measurement results for both steels are illustrated in the bar graphs of Fig. 2. The C-Mn-Nb steel exhibited a smaller ferrite grain size with lower pearlite content compared to plain C-Mn steel.

For inclusion analysis, the polished samples first were observed under an optical microscope and classified on the basis of their reflectivity/color and morphology. Light gray elongated inclusions and dark globular inclusions were visible in both steels. Subsequent SEM/EDX analysis confirmed that the majority of the elongated inclusions were manganese sulfides (Fig. 3) and that the dark globular inclusions were alumina oxides (Fig. 4). Various inclusion parameters such as length, width, aspect ratio, and volume fraction of the elongated sulfides and globular or stringer oxides were also obtained using an image analyzer. Typical video-optical micrographs showing inclusion distribution in polished samples of both steels are presented in Fig. 5. Size distribution of the sulfide and oxide in-

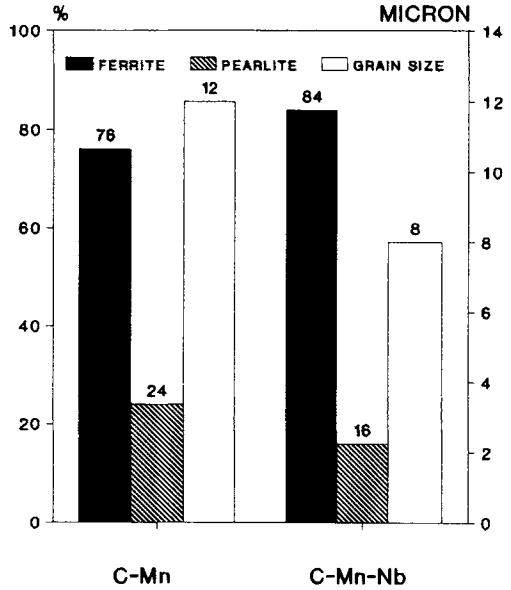

Fig. 2 Area fraction of ferrite and pearlite and ferrite grain size in the C-Mn and C-Mn-Nb steels

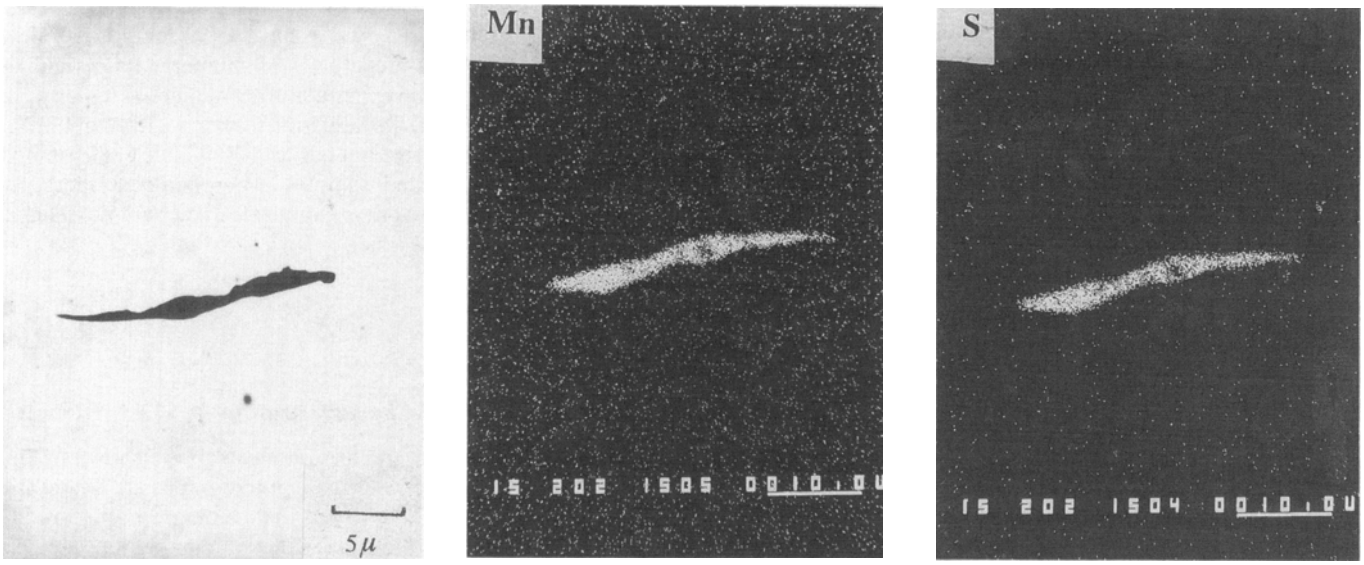

(a) (b) (c)

Fig. 3 SEM/x-ray mapping showing the presence of elongated manganese sulfide inclusions in the C-Mn steel

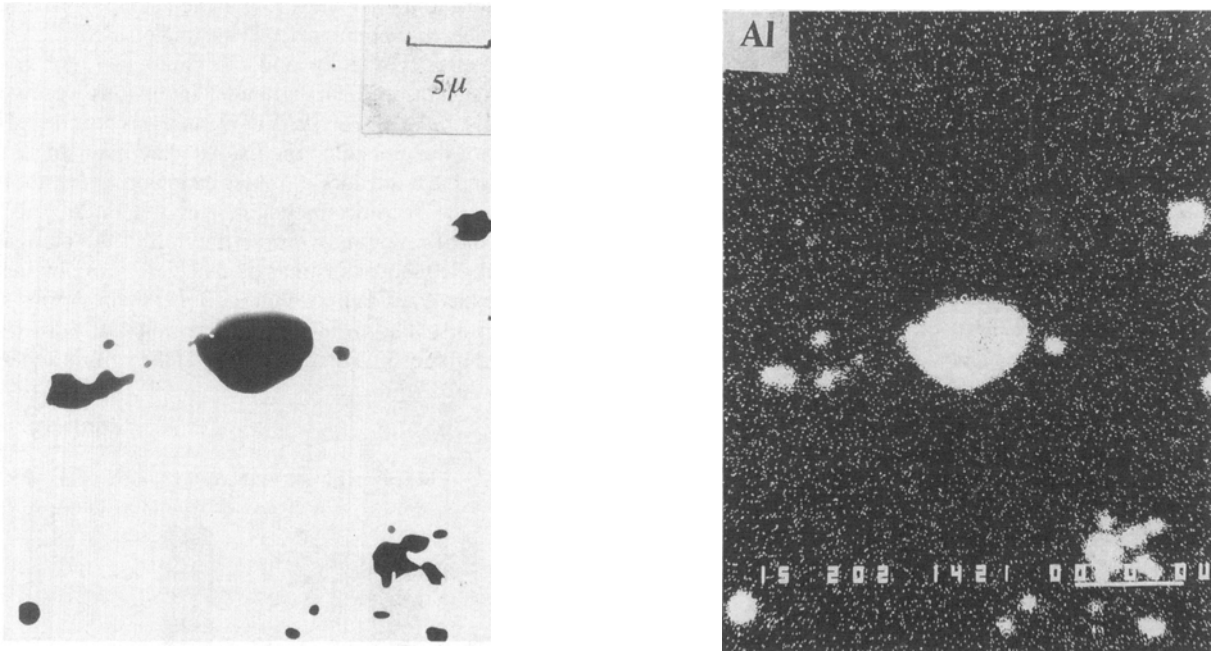

(a) (b)

Fig. 4 SEM/x-ray mapping showing the presence of globular alumina oxide inclusions in the C-Mn steel

clusions in both steels is shown in Fig. 6. Results of all these microstructural parameters are summarized in Table 2. As seen from the volume fraction measurements of both steels, the inclusion population in the C-Mn-Nb steel is smaller, which could be due to low sulfur, phosphorus, aluminum, and manganese content in this steel.

3.2 *Tensile Testing*

Tensile testing results in the form of bar graphs are shown in Fig. 7. These results are the average values of a minimum of three tests for each steel. The C-Mn-Nb steel shows a higher yield strength as well as a higher YS/UTS ratio and a lower percentage elongation compared to plain C-Mn steel.

3.3 *Charpy Impact Energy*

The DBTT curves for both steels are illustrated in Fig. 8. The impact value at each temperature is the average of at least three samples tested. The upper shelf energy value at room temperature is higher in the C-Mn-Nb steel. However, at subzero temperatures, C-Mn-Nb showed lower impact energy than

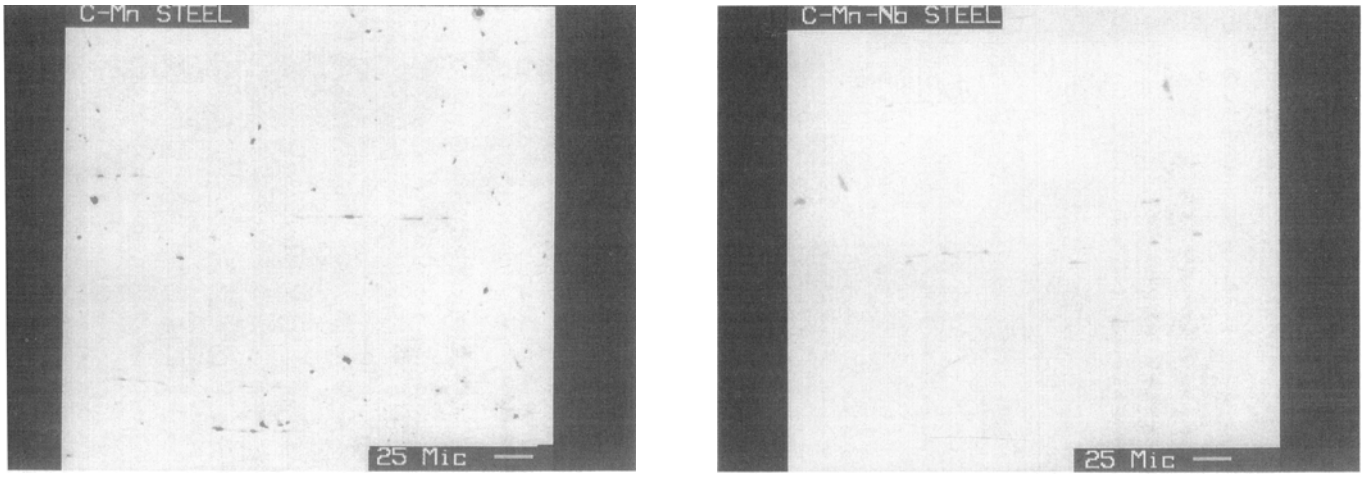

(a) (b)

Fig. 5 Video-optical micrographs showing inclusion distribution. (a) C-Mn. (b) C-Mn-Nb

plain C-Mn steel. The DBTT defined at 20 J was found to be −74 and −52 °C for C-Mn and C-Mn-Nb, respectively.

3.4 *HAZ Toughness*

Impact energy values obtained on simulated HAZ samples tested at −30 °C are shown in Fig. 9. The C-Mn-Nb steel shows lower impact values for all heat inputs. At higher heat input, the difference in impact values of the two steels is more pronounced. Microhardness measurements also show higher HAZ hardness in the C-Mn-Nb steel compared to plain C-Mn steel (Fig. 10).

4. Discussion

The major microstructural differences observed in these two steels involved pearlite banding, ferrite grain size, and volume fraction of nonmetallic inclusions. The prominent banded ferrite-pearlite structure was seen in the C-Mn steel. In general, the banded structure in steels is produced by chemical heterogeneity due to dendritic or small-scale segregation during cooling of ingots. The detailed mechanism of banded structure formation in steels is extensively discussed by Bastein (Ref 6). Most of the impurities and alloying elements result in dendritic segregation. However, the extent of such segregation depends on the nature of the element and its concentration in the steel. As reported in the literature (Ref 6), among the metals and nonmetals, manganese, carbon, phosphorus, and sulfur are considered to have a marked ability to produce banded structure due to segregation. The proportion of these elements was greater in the case of the C-Mn steel, which could be the reason for the severe banding observed in this steel.

The controlled-rolled C-Mn-Nb steel shows a finer ferrite grain size as compared to the hot-rolled and normalized plain C-Mn steel. The mechanism of achieving such fine ferrite grain size of microalloyed steels by controlled rolling has been extensively studied over the last 25 years by several investigators (Ref 7-11). It has been clearly established that at higher deformation temperatures during rolling of niobium-microalloyed steel, relatively coarse niobium carbonitride [Nb(C,N)] particles precipitate and restrict grain-boundary migration so that austenite grain growth is restricted in the niobium-microalloyed steels as compared to plain C-Mn steels. However, at lower temperatures, delay in austenite recrystallization is caused by niobium in solution in the austenite. It has also been demonstrated that niobium addition is most effective in retarding the recrystallization of austenite. Thus, both dissolved niobium and fine Nb(C,N) precipitates retard recrystallization of austenite. Further deformation of austenite accelerates nucleation of numerous strain-induced fine Nb(C,N) precipitates, which act as nuclei for austenite-to-ferrite transformation and thus promote the development of very fine ferrite grains.

To examine the microstructural features and presence of Nb(C,N) precipitates in controlled-rolled C-Mn-Nb steel, thin-foil samples were observed under the TEM. Typical TEM micrographs of this steel (Fig. 11) show fine spacing of pearlite with highly dislocated ferrite. However, the presence of fine Nb(C,N) precipitates could not be detected using the present sample preparation technique. This needs further TEM investigation using tedious chemical extraction methods and replica techniques to determine the size/shape distribution of niobium precipitates. Hence, the presence of niobium in the steel was confirmed only by repeated chemical analysis.

The finer grain size and fine Nb(C,N) precipitates are the two important strengthening parameters which contribute to the higher yield strength observed in the C-Mn-Nb steel (453 N/mm^2) compared to the C-Mn steel (350 N/mm^2). Various equations are available in the literature for determining the contribution of each parameter and predicting the yield strength of the ferrite-pearlite steels. One such equation has been proposed by Kouwenhoven (Ref 12) to predict yield strength on the basis of quantitative effects of various compositional and microstructural factors:

$$\text{YS (N/mm}^2) = 54V_f + [380 + 94\,(\%\text{Mn})]V_p + 72(\%\text{Si}) + 26(d_f)^{1/2} \quad \text{(Eq 1)}$$

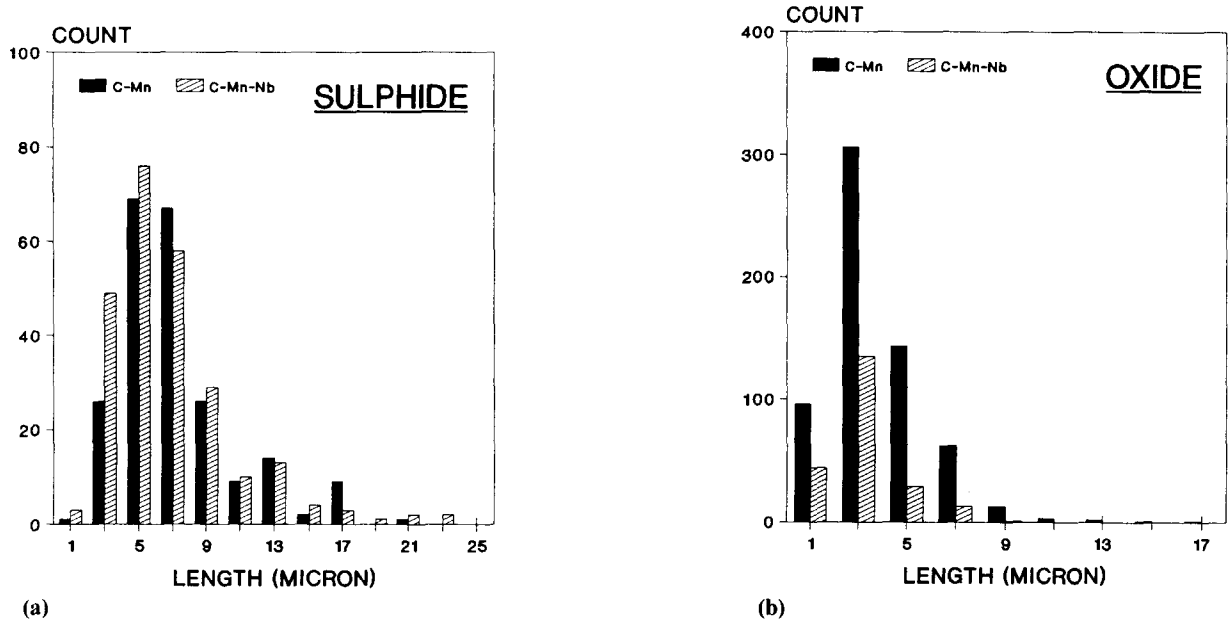

Fig. 6 Size distribution of sulfide (a) and oxide (b) inclusions in C-Mn and C-Mn-Nb steels

Table 2 Microstructural parameters

Parameter	Steel			
	C-Mn		C-Mn-Nb	
Ferrite grain size, μm	12.00 ± 2.16		8.00 ± 1.44	
Pearlite content, %	24.69 ± 4.93		16.34 ± 3.26	
Inclusion rating	Thin	Heavy	Thin	Heavy
Sulfide	0.5	...	1.0	...
Alumina	2.5	...	2.0	...
Silicate	...	...	0.5	...
Globular	4.0	...	2.0	...
Area fraction of total inclusions, %	0.10 ± 0.015		0.06 ± 0.012	
Average size of sulfide inclusions, μm	7.24 ± 3.47		6.96 ± 4.1	
Average size of oxide inclusions, μm	3.82 ± 2.1		3.38 ± 1.5	

where V_f is volume fraction of ferrite, V_p is volume fraction of pearlite, and d_f is ferrite grain size (mm). Equation 1 accounts for the strengthening contribution by lattice friction, solute elements, and grain-size effect, but does not include strengthening due to microalloying additions. Using this equation, the predicted strength of C-Mn steel was found to be 363 N/mm^2, which was slightly higher than the experimentally observed value (350 N/mm^2). However, in the case of niobium-containing steel, the predicted strength was 405 N/mm^2, which was much lower than the experimentally observed value (453 N/mm^2). This short fall in the predicted YS value of niobium-containing steel clearly implies that 0.03% Nb addition increases the strength roughly about 50 N/mm^2 due to a precipitation-hardening effect.

This precipitation-hardening effect can be predicted independently using a well-known Orowan model (Ref 13):

$$\sigma_{ppt} = C/I \quad \text{(Eq 2)}$$

where σ_{ppt} is the precipitation strengthening increment, C is a material constant, and I is interparticle spacing. Based on this model, the equation relating σ_{ppt} (ksi) with niobium (wt%) and precipitate size, D (Å), was found to be (Ref 14)

$$\sigma_{ppt} = [1000/D][(\text{Nb})^{1.3} - 0.12] \quad \text{(Eq 3)}$$

Equation 3 predicts the strengthening power of niobium at different precipitate sizes.

The Orowan model was subsequently modified by Ashby (Ref 15). Based on this Ashby-Orowan model, work of Gladman et al. (Ref 16) has shown that σ_{ppt} (MPa) is related to volume fraction of fine precipitate, f, and mean planar-intercept diameter of precipitates, $X_{(mm)}$, as:

$$\sigma_{ppt} = [(5.9\sqrt{f}/X)][\ln(X/\mathbf{b})] \quad \text{(Eq 4)}$$

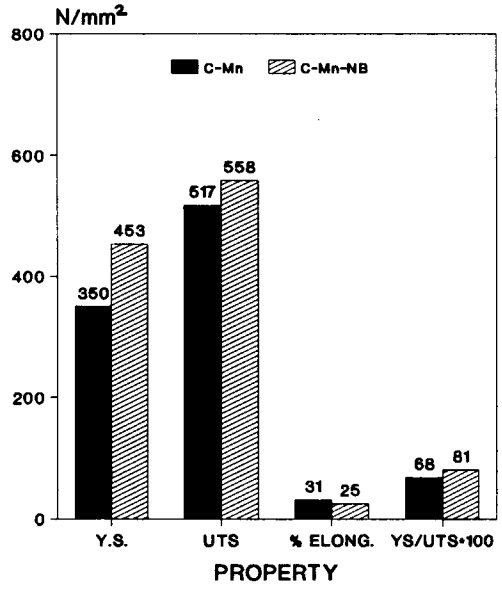

Fig. 7 Influence of niobium microalloying on tensile properties

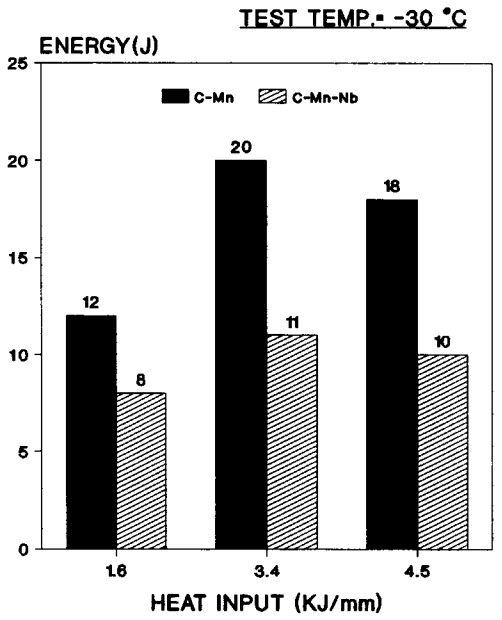

Fig. 9 Influence of niobium microalloying on HAZ toughness with different heat inputs

where **b** is the Burger's vector in the slip direction, which is 2.5 Å for ferrite, and the mean planar-intercept diameter, X, is related to the mean precipitate diameter, D, observed in a thin-foil specimen (Ref 17) as:

$$X = D(\sqrt{2/3})$$

A close agreement between precipitation strengthening indicated by the difference between the observed yield strength and the value predicted by Eq 1 and the value predicted by Eq 4 is reported by Gladman et al. (Ref 16).

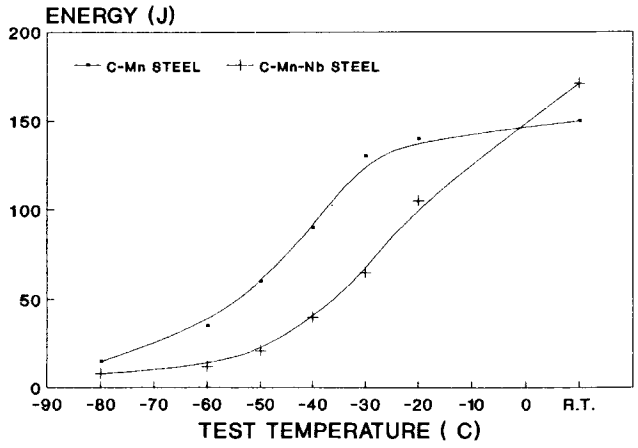

Fig. 8 Influence of niobium microalloying on DBTT

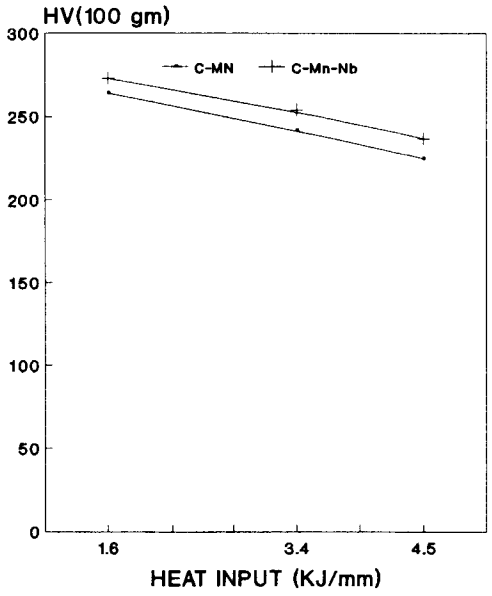

Fig. 10 Variation of microhardness as a function of niobium and heat input

The increased yield strength due to niobium addition in the steel has an adverse effect on plastic deformation characteristics. This has been reflected in a lower value of the percentage elongation and a higher YS/UTS ratio of the niobium-containing steel. Since both these parameters control the formability of the steel, it is important that they have optimum values. The low strain-hardening properties related to a high YS/UTS ratio are sometimes considered to indicate a low energy absorption potential of the steel and therefore a higher risk of failure. Thus, some rules exclude the use of microalloyed steels having a YS/UTS ratio higher than 0.75 (Ref 18). The present trend in alloy design (as applicable to C-Mn-Nb steel) toward increased yield strength, better notch toughness, and lower carbon equivalent for improved weldability leads to a higher YS/UTS ratio, particularly when the carbon content is low. Hence, a carbon content of 0.15 to 0.16% is desirable in the steel to maintain an optimum YS/UTS ratio. In this re-

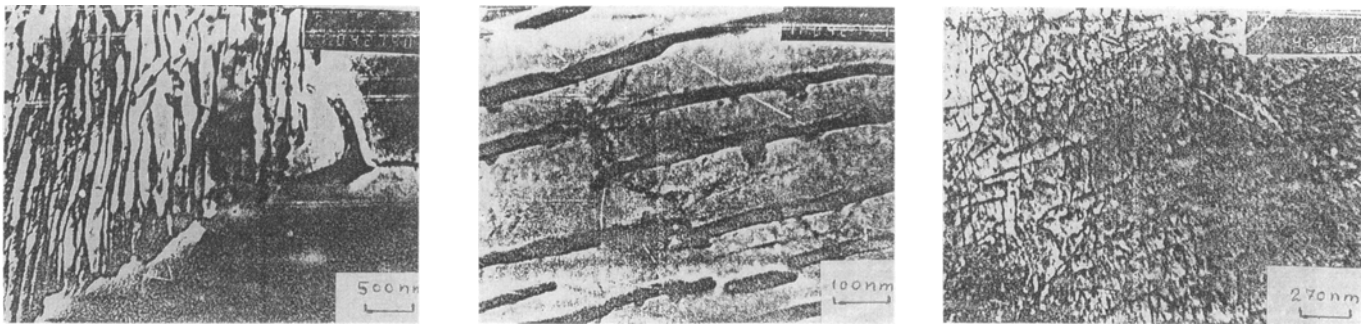

(a) (b) (c)

Fig. 11 TEM micrographs of C-Mn-Nb steel. (a) Ferrite and pearlite. (b) Fine spacing of pearlite. (c) Highly dislocated ferrite

(a) (b) (c)

Fig. 12 Video-optical micrographs of simulated HAZ samples of C-Mn steel at different heat inputs. (a) 1.6 kJ/mm. (b) 3.4 kJ/mm. (c) 4.5 kJ/mm

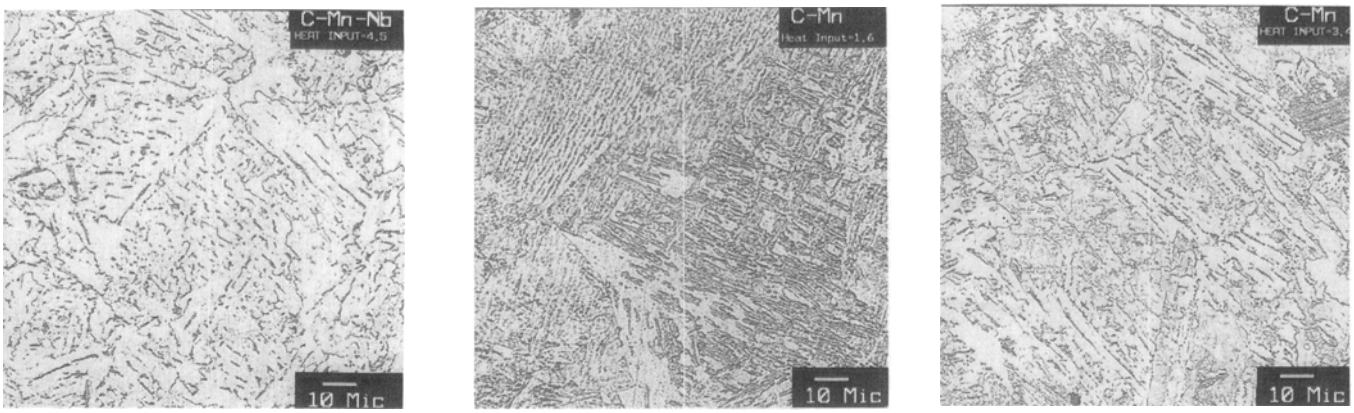

(a) (b) (c)

Fig. 13 Video-optical micrographs of simulated HAZ samples of C-Mn-Nb steel at different heat inputs. (a) 1.6 kJ/mm. (b) 3.4 kJ/mm. (c) 4.5 kJ/mm

spect, C-Mn steel seems to be a safer choice than niobium-microalloyed steel as a ship hull construction material.

As has been shown, the two factors governing the strength of the niobium-added steel are grain size and carbide/carbonitride dispersion hardening. When impact properties are considered, the picture becomes more complicated. As Fig. 8 shows, the DBTT of C-Mn-Nb steel (–52 °C) is higher by about 22 °C than plain C-Mn steel (–74 °C). It was expected that the niobium-added steel would produce a lower DBTT since it has a lower inclusion content and finer ferrite grain size. Earlier works of various investigators (Ref 19-22) recognized the role of inclusions in reducing the ductility and toughness of various

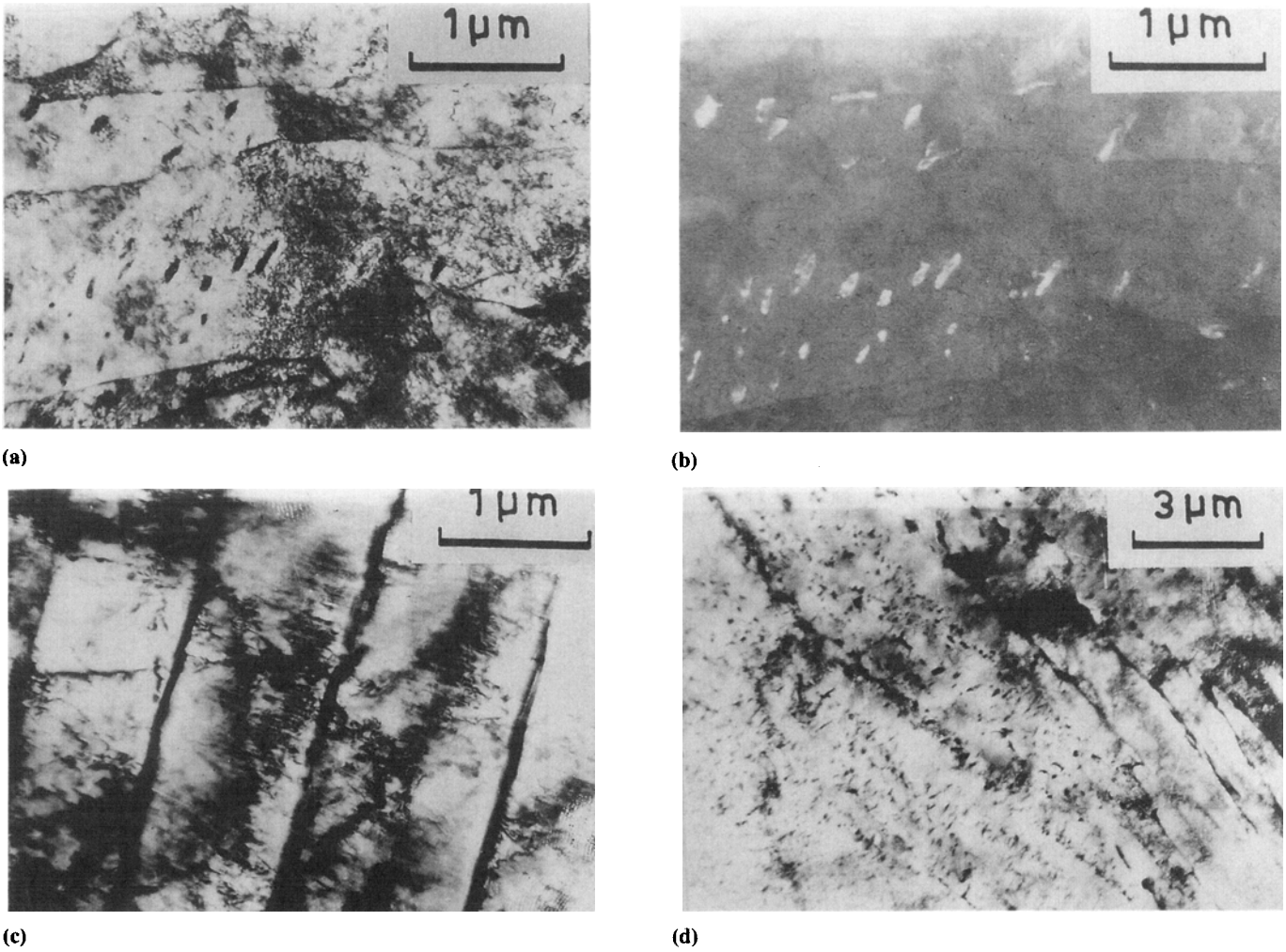

Fig. 14 TEM micrographs of simulated HAZ region at 1.6 kJ/mm. (a) and (b) C-Mn steel. (c) and (d) C-Mn-Nb steel

steels. The detrimental effect of sulfide inclusions is also clearly shown in recently published work (Ref 23). Similarly, the strong influence of grain size on impact transition temperature is reported by Petch (Ref 24), who has shown that for each unit increase in $d^{-1/2}$ ($mm^{-1/2}$), the transition temperature is decreased by 11.5 °C. Since our results show a low volume fraction of inclusions and fine ferrite grain size in the case of the C-Mn-Nb steel, this should have improved the low-temperature notch toughness of the material. However, the results indicate the adverse effect of strengthening due to Nb(C,N) precipitation on DBTT, which counteracts the favorable effect of low inclusion content and fine grain size. The net result of these factors is a positive rise in DBTT in the case of niobium-added steel.

The detailed work carried out by Morrison and Woodhead (Ref 25) on the effect of niobium on impact transition temperature suggested that the precipitation of Nb(C,N) in the austenite reduces the ferrite grain size and also increases the resistance of ferrite lattice to plastic deformation (σ_i) and dislocation locking stress parameter (K_y). Both σ_i and K_y are dependent on the amount of precipitates and elements in solid solution of ferrite. However, their results did not enable the authors to distinguish between the two effects. Subsequently, Morrison (Ref 26) has indicated that only σ_i is affected by niobium addition; this was further confirmed by the extensive work of Phillips et al. (Ref 27). Therefore, the major effect of niobium addition on impact properties is by precipitation of fine Nb(C,N) and not as a solid-solution hardener. Thus, niobium addition, although it refines ferrite grain size, has a detrimental effect on impact transition temperature by increasing the resistance of ferrite lattice to plastic deformation. Our results are also in accordance with earlier researchers (Ref 28, 29) who reported that the fine carbonitride precipitates of niobium or vanadium increase the impact transition temperature by about 0.3 to 0.5 °C for each 1 MPa increase in yield stress by precipitation strengthening.

Charpy testing at –30 °C of simulated HAZ specimens also shows lower impact values in niobium-added steel. Optical microscopic studies of simulated HAZ regions of both steels showed upper bainite as dominant microstructural constituent, with colonies of parallel ferrite plates containing thin, elongated, dark carbides. Video-optical micrographs of HAZ regions of plain C-Mn and C-Mn-Nb steels for different heat inputs showing these features are presented in Fig. 12 and 13, respectively. To gain further details of microstructural features, TEM studies on simulated HAZ regions were carried out. Transmission electron micrographs at different heat inputs for

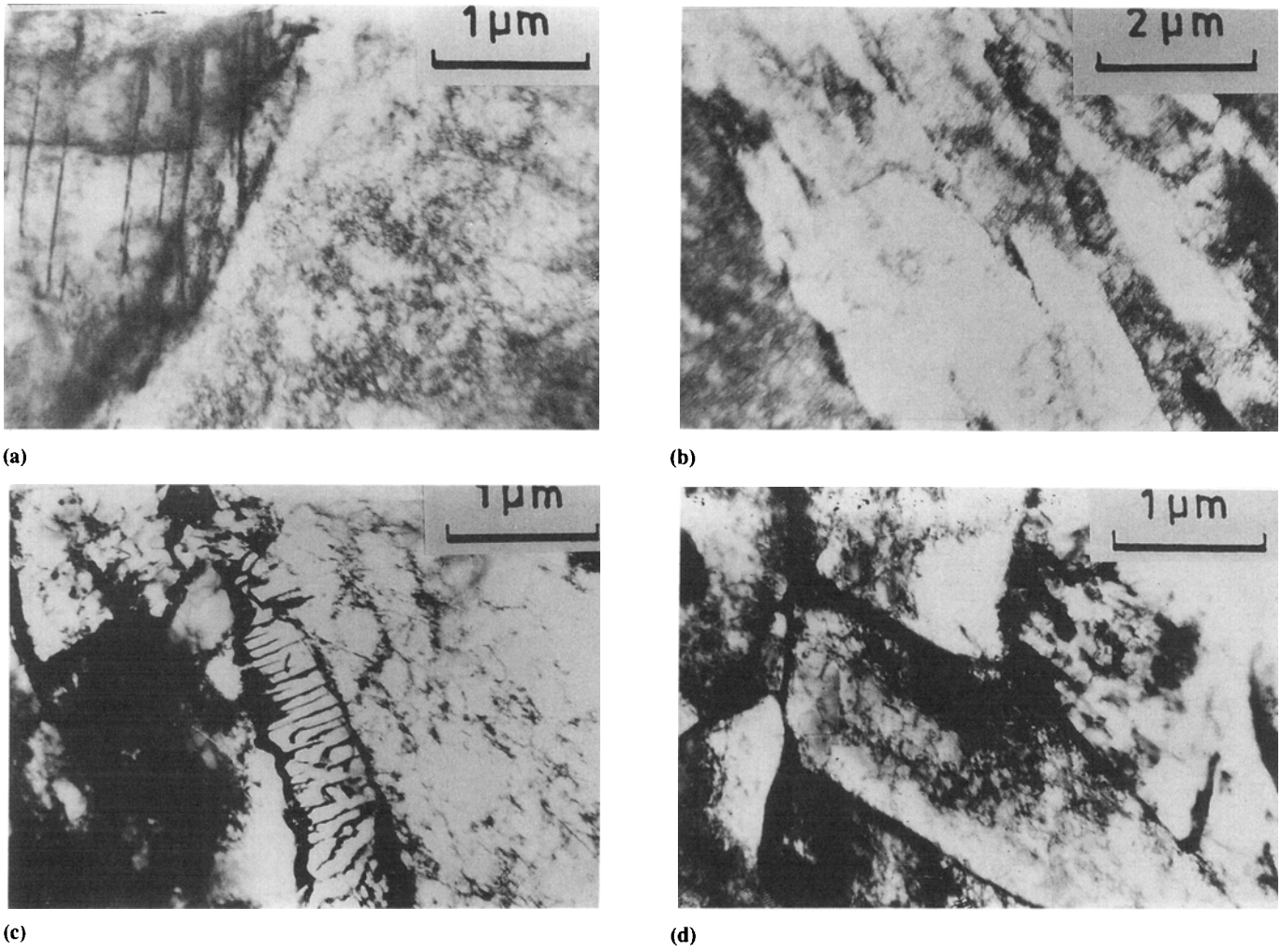

Fig. 15 TEM micrographs of simulated HAZ region at 3.4 kJ/mm. (a) and (b) C-Mn steel. (c) and (d) C-Mn-Nb steel

both steels are illustrated in Fig. 14 to 16. This study clearly revealed that at lower heat input (1.6 kJ/mm)—that is, at a faster cooling rate—both steels show mixed upper and lower bainitic structure. Characteristics of upper bainitic structure with interlath cementite film or spheroids at the ferrite lath boundaries and lower bainite with intralath cementite are seen in Fig. 14. In addition to cementite spheroids, the presence of very fine Nb(C,N) precipitates are also visible in the case of niobium-added steel (Fig. 14c).

At higher heat input (3.4 and 4.5 kJ/mm)—that is, at a slower cooling rate—both steels show the presence of pearlitic-bainitic structure. However, in the case of niobium-added steel, the presence of some dark regions was also evident, which could be islands of martensite (Fig. 15d). Also, the niobium-added steel showed the presence of cementite at the ferrite grain boundary as well as fine Nb(C,N) precipitates at the dislocated substructure within ferrite grains (Fig. 16c). These features in the case of niobium-added steel also resulted in higher microhardness values in the HAZ region compared to plain C-Mn steel. Thus, the HAZ toughness reduction in niobium-added steel, particularly at higher heat input, is because of the mixed pearlitic-bainitic-martensitic structure having higher hardness due to the added effect of precipitation hardening.

Further research is in progress on controlled rolling coupled with controlled cooling of niobium-microalloyed steel to achieve favorable size/shape distribution of Nb(C,N) precipitates. This may help to improve the DBTT and HAZ toughness properties of niobium-microalloyed steel.

5. Conclusions

- Niobium microaddition in the controlled rolled C-Mn steel results in higher yield strength due to the precipitation of fine niobium carbonitrides.
- High ductile-brittle transition temperature (DBTT at 20 J) in the case of niobium-added steel is due to the adverse effect of precipitation strengthening, nullifying the favorable effect of fine grain size and lower inclusion and pearlite contents on DBTT.
- Heat-affected zone toughness reduction in C-Mn-Nb steel is due to the presence of an upper bainitic structure with martensitic islands that possess higher hardness due to the added effect of precipitation strengthening.

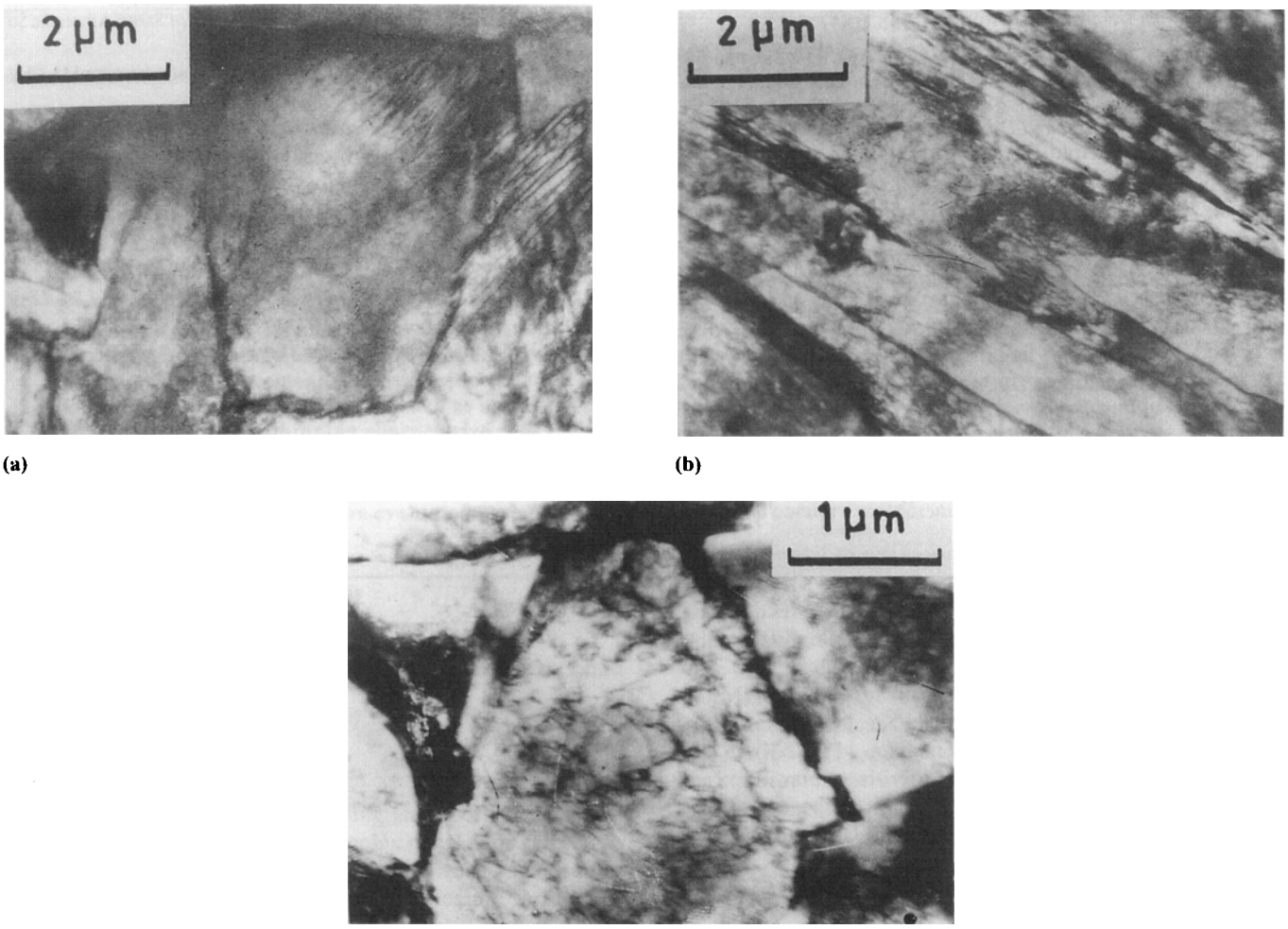

(a) (b) (c)

Fig. 16 TEM micrographs of simulated HAZ region at 4.5 kJ/mm. (a) and (b) C-Mn steel. (c) C-Mn-Nb steel

Acknowledgments

The authors wish to thank Dr. P.C. Deb, Director, Naval Chemical & Metallurgical Laboratory (Bombay) for his continued support and encouragement during this research work and for his permission to publish this paper. They also wish to thank the authorities of the Metallurgical Engineering Department, Banaras Hindu University (Varanasi), for extending their TEM facilities.

References

1. *Microalloying*, *75*, American Society for Metals, 1975
2. *Welding of HSLA (Microalloyed) Structural Steels*, A.B Royhwell and J.M. Gray, Ed., American Society for Metals, 1976
3. D.E. Passoja and J.R. Strife, Electron Microscopy—Closing the Structure-Property Gap, *J. Met.*, Feb 1977, p 12
4. "Standard Methods of Tension Testing of Metallic Materials," E 8, *Annual Book of ASTM Standards*, Vol 03.01, ASTM, 1984, p 130
5. "Standard Methods of Notched Bar Impact Testing of Metallic Materials," E 23, *Annual Book of ASTM Standards*, Vol 03.01, ASTM, 1984, p 210
6. P.G. Bastein, *J. Iron Steel Inst. (Lond.)*, Vol 187, 1957, p 281
7. G.R. Speich, L.J. Cuddy, L.R. Gorden, and A.J. DeArdo, *Proc. Int. Conf. Phase Transformation in Ferrous Alloys*, A.R. Marder and J.I. Goldstein, Ed., AIME, 1983, p 341
8. I. Tamura, H. Sekine, and T. Tanaka, *Thermomechanical Processing of High Strength-Low Alloy Steels*, Butterworths, London, 1988, p 20
9. Y. Saito, C. Shiga, and T. Emani, *Proc. Int. Conf. Physical Metallurgy of Thermomechanical Processing of Steels and Other Metals*, I. Tamura, Ed., ISIJ, 1988, p 753
10. E.J. Palmiere, C.I. Garcia, and A.J. DeArdo, *Proc. Int. Conf. Processing, Microstructure & Properties of Microalloyed and Other Modern High Strength Low Alloy Steels*, A.J. DeArdo, Ed., AIME, 1991, p 113
11. A.C. Kneissl, C.I. Garcia, and A.J. DeArdo, *Proc. Int. Conf. Processing, Microstructure & Properties of Microalloyed and Other Modern High Strength Low Alloy Steels*, A.J. DeArdo, Ed., AIME, 1991, p 145
12. H.J. Kouwenhoven, *Trans. ASM*, Vol 62, 1969, p 437
13. E. Orowan, *Internal Stress in Metals and Alloys*, Institute of Metals, London, 1948, p 451
14. R.B.G. Yeo, A.G. Melville, P.E. Repas, and J.M. Gray, *J. Met.*, Vol 20, June 1968, p 33
15. M.F. Ashby, *Oxide Dispersion Strengthening*, AIME, 1966, p 143
16. T. Gladman, D. Dulieu, and I.D. McIvor, *Microalloying '75*, American Society for Metals, 1975, p 32

17. R.L. Fullman, *Trans. AIME*, Vol 197, 1953, p 447

18. A. Kothe, J. Richter, A. Guth, L. Kaun, G. Backmann, M. Schaper, and V. Gutteck, Recrystallisation of C-Si-Mn-Ti-V-Nb Steel Plate, *Proc. Int. Conf. Processing, Microstructure & Properties of Microalloyed and Other Modern High Strength Low Alloy Steels*, A.J. DeArdo, Ed., AIME, 1991, p 461

19. T.J. Baker and J.A. Charles, *The Effect of Second Phase Particles on the Mechanical Properties of Steel*, Iron and Steel Institute, London, 1971, p 79

20. A.J. Birkle, R.P. Wei, and G.E. Pellisier, *Trans. ASM*, Vol 59, 1966, p 981

21. T. Gladman, B. Homes, and F.B. Pickering, *J. Iron Steel Inst. (Lond.)*, Vol 298, 1970, p 172

22. I. Kozasu and J. Tanaka, *Sulfide Inclusions in Steel*, American Society for Metals, 1975, p 286

23. D.K. Biswas, C.S. Narendranath, M. Venkatraman, and U. Chatterjee, *Metall. Trans.*, May 1992, p 1479

24. N.J. Petch, *Proc. Swampscott Conf.*, MIT Press, 1959, p 54

25. W.B. Morrison and J.H. Woodhead, *J. Iron Steel Inst. (Lond.)*, Vol 201, 1963, p 43

26. W.B. Morrison, *J. Iron Steel Inst. (Lond.)*, Vol 201, 1963, p 317

27. R. Phillips, W.E. Duckworth, and F.E.L. Copley, *J. Iron Steel Inst. (Lond.)*, Vol 202, 1964, p 593

28. K.J. Irvine, F.B. Pickering, and T. Gladman, *J. Iron Steel Inst. (Lond.)*, Vol 205, 1967, p 161

29. T. Gladman, *J. Iron Steel Inst. (Lond.)*, Vol 203, 1965, p 1038